Energy flow analysis for curved beams

A. Le Bot, M. N. Ichchou, and L. Jezequel
Laboratoire de Tribologie et Dynamique des Systèmes, UMR CNRS 5513, École Centrale de Lyon 36, avenue Guy de Collongues, BP163, 69131 Ecully cedex France

(Received 25 July 1995; revised 4 November 1996; accepted 31 March 1997)

This paper presents an energy model for the medium- and high-frequency analysis of Love–Kirchhoff curved beams. This model introduced by Nefske and Sung [Statistical Energy Analysis NCA **3**, 47–54 (1987)] for straight beams and investigated further by other authors, is developed for curved rods (tangential or longitudinal waves), and then for curved beams (radial or flexural waves). The exact-energy solution for curved rods or beams is shown to consist of a smooth spatial variation, which the energy model represents, and a spatially oscillating solution, which can be represented by an energy envelope. Finally, a complete energy model is proposed for curved components including both longitudinal and flexural waves. Boundary conditions are also given in this paper. It is shown that this method, which is numerically attractive in the mid- and high-frequency range, predicts the arithmetic mean value of the energy variables. © *1997 Acoustical Society of America.* [S0001-4966(97)05807-4]

PACS numbers: 43.40.Cw [CBB]

LIST OF SYMBOLS

ω	circular frequency
E_0	Young's modulus
E	complex modulus
η	damping ratio
s	curvilinear coordinate
R	radius of curvature
S	area of section
I	inertia
ρ	mass density
N	tensile load
T	shear force
M	bending moment
u	tangential displacement
v	radial displacement
θ	rotation of section
W	energy density
P	active energy flow
p_{diss}	power density being dissipated
p_{lf}	exchanged power density from longitudinal to flexural form
k	complex wave number of curved system
k_∞	complex wave number of straight system
c_g	group velocity
a^+, a^-, b^+, b^-	displacement magnitudes
A^+, A^-	energy magnitudes

INTRODUCTION

In designing structures, one of the main questions is how to predict and control noise and vibration? At low frequencies, several tools allow the vibration level and the noise transmission to be predicted so that effective treatments can be applied. Among these techniques, the finite element method and the boundary element method are at present the most important ones. However, these methods are not suited to the analysis of the behaviour of systems in the mid- and high-frequency range, because a small mesh size is required which makes model generation, turnaround time, and computations too costly.

At high frequencies where the modal density of structures is relatively high, statistical energy analysis (SEA)[1] is often used to predict the space and frequency-averaged energy level of each component of a built-up structure. However, the SEA method gives no information on the spatial repartition of energies within each substructure. In addition, SEA requires the use of coupling loss factors which are difficult to predict for complex structures.

Concerning the dynamic analysis of structures in the mid- and high-frequency range, some methods are still based upon the modal behavior. Dowell and Kubota[2] and Doherty and Dowell[3] have shown that some results of SEA can be derived from an asymptotic limit of classical modal analysis. They called this approach the asymptotic modal analysis (AMA). This technique is based on the assumptions that in the frequency domain under consideration, the modal characteristics such as masses, frequencies, and damping, do not vary rapidly. Thus at high frequencies, AMA can be used to predict frequency-averaged vibrational responses. However, the feasibility of this technique for the analysis of complex structures has yet to be demonstrated.

In an another context, Guyader[4] developed the so-called modal sampling method (MSM) for single and coupled rods. It consists of retaining only the most energetic modes in the modal decomposition of the structural response. Then, the method allows the prediction of an average level of structural response. This technique is still under development.

The power flow method presented by Belov *et al.*[5] and Luzzato[6] would appear to be an interesting alternative for use in the mid- and high-frequency range. This approach takes into account the spatial variation of energy within systems and is an analytical formulation. In addition it is amenable to

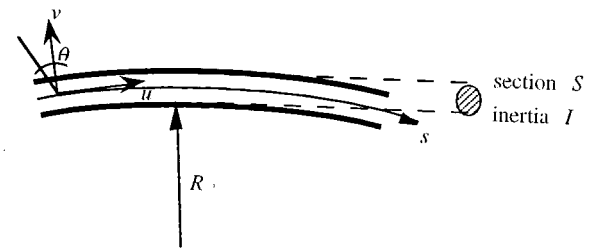

FIG. 1. Naturally curved beam.

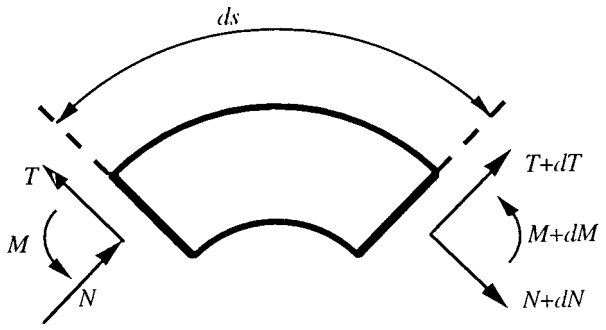

FIG. 2. Differential element from a curved beam.

a numerical implementation such as finite or boundary element methods. Nefske and Sung[7] established the relation between the energy density and its flow in beams, and wrote a second-order differential equation similar to that which describes heat conduction. Wohlever and Bernhard,[8] and Bouthier and Bernhard[9,10] investigated the procedure further. They proposed an energy model for bars, beams, membranes, plates, and acoustical cavities. The cases considered involved a single mode of propagation (unique group velocity), and a single form of energy.

The aim of this study is to present an energy model of Love–Kirchhoff curved beams.[11] First, the equation of motion is established in terms of radial and tangential displacement of a curved beam. The expressions of the total energy density and the energy flow are also provided. Energy equation and boundary conditions are developed separately for flexural and longitudinal waves. Finally, a complete energy model for curved beams including both flexural and longitudinal effects is given. A numerical example is presented to show the feasibility of this method.

I. KINEMATIC MODEL FOR CURVED BEAMS

The addition of curvature to beams which leads to an infinite variety of shapes, significantly modifies the vibrational behavior of beams. The standard reference for the governing equations of beams of arbitrary curvature is Love.[11] Referring to Love, the dynamical equation of motion for a beam of constant curvature is presented with several simplifications. Energy quantities are also given.

First of all, the curved beam is assumed to be excited by a harmonic pure tone $f=\omega/2\pi$ and steady state conditions are assumed. Therefore, by using complex notation, the time dependence $e^{i\omega t}$ is suppressed in the remaining text. A hysteretic damping model is adopted. Thus a complex modulus $E=E_0(1+i\eta)$ is introduced where E_0 is the Young's modulus.

Consider the curved beam shown in Fig. 1. The kinematic behavior depends on the displacement of each section. Three degrees of freedom are needed to describe displacements. The tangential displacement along the neutral axis s of the beam is denoted by u, and ν and θ denote the radial displacement and the rotation, respectively, of each section. The tensile load is noted N, the shear force T, and the bending moment M. The variations of these quantities are shown for a positive increment of arc length ds in Fig. 2.

The dynamic equilibrium of the element is then written in the three directions of displacement:

$$R\frac{dN}{ds}+T=-\rho SR\omega^2 u,$$

$$R\frac{dT}{ds}-N=-\rho SR\omega^2 \nu, \tag{1}$$

$$\frac{dM}{ds}+T=-\rho I\omega^2\theta.$$

It can be also shown[11] that the relationships between the tensile load N, the bending moment M, and the displacements are as follows:

$$N=ES\left(\frac{\nu}{R}+\frac{du}{ds}\right),\quad M=EI\frac{d}{ds}\left(-\frac{u}{R}+\theta\right). \tag{2}$$

In addition, assuming that the plane sections remain orthogonal to the neutral axis, the relationship which relates the degree of freedom θ to the radial displacement ν is simply

$$\theta=\frac{d\nu}{ds}. \tag{3}$$

By neglecting the inertia term of rotation in the momentum equilibrium relationship (1), and by combining the expressions (1)–(3), the governing equations of a curved beam under steady state conditions, become

$$EI\frac{d^2}{ds^2}\left(\frac{u}{R}-\frac{d\nu}{ds}\right)+ES\frac{d}{ds}\left(\nu+R\frac{du}{ds}\right)=-\rho RS\omega^2 u,$$

$$EI\frac{d^3}{ds^3}\left(\frac{u}{R}-\frac{d\nu}{ds}\right)-ES\left(\frac{\nu}{R^2}+\frac{1}{R}\frac{du}{ds}\right)=-\rho S\omega^2\nu. \tag{4}$$

For the following developments, the propagation characteristics are obtained for such structures, by considering harmonic waves of the form

$$u=ae^{-iks},\quad \nu=be^{-iks}. \tag{5}$$

By introducing these expressions into the governing equations (4), the following matrix equation is obtained:

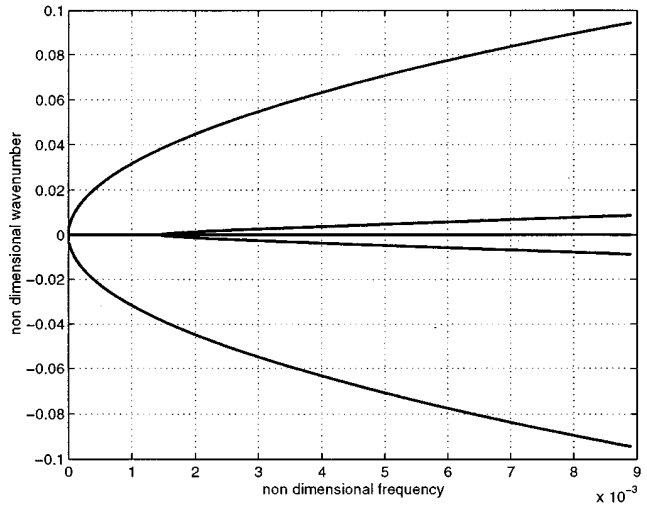

FIG. 3. Dispersion curve of a curved beam: nondimensional wave number $\overline{k}$ versus nondimensional frequency $\overline{\omega}$ for $\overline{\epsilon}=0.0014$.

$$\begin{bmatrix} \frac{\omega^2R^2}{c_0^2}-k^2R^2-k^2\mu^2 & -i(kR+k^3R\mu^2) \\ i(kR+k^3R\mu^2) & \frac{\omega^2R^2}{c_0^2}-1-k^4R^2\mu^2 \end{bmatrix} \begin{bmatrix} a \\ b \end{bmatrix} = \begin{bmatrix} 0 \\ 0 \end{bmatrix}, \tag{6}$$

where $c_0 \overset{\text{def}}{=} \sqrt{E/\rho}$ and $\mu \overset{\text{def}}{=} \sqrt{I/S}$.

Freely propagating harmonic waves may exist only if the determinant in the above system vanishes. The resulting dispersion equation is

$$\left(\frac{\omega^2R^2}{c_0^2}-k^2R^2-k^2\mu^2\right)\left(\frac{\omega^2R^2}{c_0^2}-1-k^4R^2\mu^2\right) -(kR+k^3R\mu^2)^2=0. \tag{7}$$

This bicubic equation, where the unknown is k, leads to six complex solutions where three wave numbers have opposite signs. The explicit expressions for these complex wave numbers can be obtained by using the Cardan formulas, but they are not given here for the sake of simplicity. However, some asymptotic expressions are derived for small values of $\overline{\epsilon}=\mu/R$ in Appendix A. The real parts of the nondimensional wave numbers $\overline{k}=k\mu$ deduced from the dispersion equation are plotted in Fig. 3 versus nondimensional frequency $\overline{\omega}=\mu\omega/c_0$. This curve depends on the nondimensional parameter $\overline{\epsilon}=\mu/R$ and shows the existence of two different regions. In the first region, there are two symmetric branches of propagation, while in the second region four propagating modes are exhibited. These remarks will be very useful for the wave analysis given below. We are interested in modeling at medium- and high-frequencies in the second region.

The wave number solutions of (7) can be noted as follows:

$$k_l, -k_l, k_f^p, -k_f^p, k_f^e, -k_f^e, \tag{8}$$

where the subscript l refers to longitudinal waves and f to flexural waves. In addition, the superscript p refers to propagating waves while e refers to evanescent waves. In Appendix A, it can be seen that, when the radius of curvature R becomes very large (i.e., R tends to infinity), the solutions in Eq. (8) become

$$\omega\sqrt{\frac{\rho}{E}}, -\omega\sqrt{\frac{\rho}{E}}, \left(\frac{\rho S}{EI}\omega^2\right)^{1/4}, -\left(\frac{\rho S}{EI}\omega^2\right)^{1/4}, i\left(\frac{\rho S}{EI}\omega^2\right)^{1/4}, -i\left(\frac{\rho S}{EI}\omega^2\right)^{1/4}. \tag{9}$$

These expressions are the wave numbers for longitudinal motion of bars and transverse motion of Euler–Bernoulli straight beams. This justifies the use of the subscript l and f.

The total energy density is the sum of energies associated with the longitudinal and flexural motions, as follows:

$$W_l=\frac{\rho S\omega^2}{4}uu^*+\frac{E_0S}{4}\left(\frac{\nu}{R}+\frac{du}{ds}\right)\left(\frac{\nu}{R}+\frac{du}{ds}\right)^*, \qquad W_f=\frac{\rho S\omega^2}{4}\nu\nu^*+\frac{E_0I}{4}\frac{d}{ds}\left(\frac{u}{R}-\frac{d\nu}{ds}\right)\frac{d}{ds}\left(\frac{u}{R}-\frac{d\nu}{ds}\right)^*. \tag{10}$$

Moreover, there are three kinds of active energy flow which represent the flexural and longitudinal behavior, and the energy flow density exchanged between tangential (longitudinal) and radial (flexural) waves, respectively,

$$P_l=\mathrm{Real}\left(\frac{i\omega}{2}\left\{N-\frac{M}{R}\right\}u^*\right), \qquad P_f=\mathrm{Real}\left(\frac{i\omega}{2}\left\{T\nu^*+M\frac{d\nu^*}{ds}\right\}\right), \qquad p_{lf}=\mathrm{Real}\left(\frac{i\omega}{2R}\left\{N\nu^*+M\frac{du^*}{ds}\right\}\right), \qquad p_{fl}=-p_{lf}. \tag{11}$$

In the following sections, several energy models will be presented. The aim of these models is to be able to predict the energy quantities that incorporate several simplifications without the need to solve the dynamical equations of motion (4).

II. PREAMBLE FOR THE ENERGY MODELS

We now present the smooth energy formulation (SEF) for curved beams. This approach is based on the following assumptions:

(1) The damping loss factor is small ($\eta \ll 1$).
(2) The participation of evanescent waves can be neglected.
(3) The interferences between propagating waves can be neglected.

Two energy variables are involved in these models: the energy density W defined as the sum of the kinetic energy density and the potential energy density, and the active energy flow P defined as the real part of the complex energy flow. As in previous section, a subscript is added that refers to the type of wave: l for longitudinal and f for flexural. Moreover, a superscript $+$ or $-$ denotes the direction of propagation of the wave at hand. We define the incident

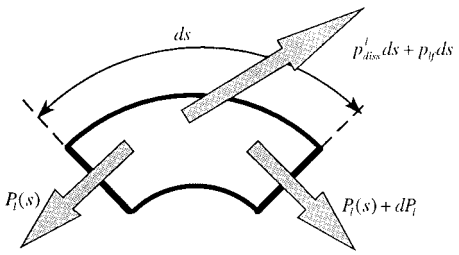

FIG. 4. Local power balance.

energy density W^+ (resp. reflected energy density W^-) and the incident energy flow P^+ (esp. reflected energy flow P^-) as the energy quantities supported by a simple incident wave (resp. reflected wave), traveling in a positive (resp. negative) direction. These quantities are sometimes called partial energies.

Obviously, when an incident wave and a reflected wave occur simultaneously, the global energy density W and the energy flow P are not *a priori* simply the sum of the corresponding partial energies. An additional term appears because of the existence of interferences between the two waves. As the smooth energy formulation (SEF) does not take into account those interferences, this additional term is neglected and the global energy density W and the active energy flow P are given in the following form:

$$P = P^+ + P^-, \quad W = W^+ + W^-. \tag{12}$$

This is a linear superposition principle extended to energy quantities.

In the following sections three energy models are studied. The first one considers just the longitudinal energies produced by a tangential wave where the effect of flexural energies is neglected. The second one considers just the flexural energies produced by a flexural wave. Finally, the third one is the most complete and takes into account the effects of the exchange of energy between the flexural and the longitudinal waves. Indeed, the previous kinematic equations show that if a longitudinal wave or a flexural wave appear alone, both longitudinal and flexural energies are produced. The two first models must not be considered as particular cases of the third but actually as an illustration. However, this approximation is introduced for the simplification that it brings. As can be seen, the power exchanged between the two waves is not high especially at high frequencies. If a given system is excited with a tangential force or with a radial force, the corresponding energy dominates and the other energy may be neglected.

III. ENERGY MODEL FOR TANGENTIAL WAVE

A. Energy flow equation

Consider a system subjected to only longitudinal vibrations. The energy quantities associated with this wave are denoted as W_l and P_l.

The first step in the derivation of the energy models is the well-known local power balance (Fig. 4). Under steady state conditions with no load, the global power balance becomes

$$\frac{dP_l}{ds} + p^l_{\text{diss}} + p_{lf} = 0 \quad \text{with} \quad p^l_{\text{diss}} = \eta\omega W_l \quad \text{and} \quad p_{lf} = a_l W_l. \tag{13}$$

The second relationship (13) is a common model for dissipation. For instance, this is precisely the model used in statistical energy analysis.[1] It assumes no distinction between kinetic and potential energy densities. While the third relationship (13) is the part of longitudinal energy transferred to flexural energy, flexural energy is not taken into account in this model, and may be considered as a dissipative term.

Hence, in order to establish an explicit energy equation, a relationship between the global active energy flow and the total energy density $P_l = H(W_l)$ has to be obtained. This relationship depends on the kind and the number of the waves that occur which, in this section, is just the longitudinal wave. It is not easy to exhibit the more general energy operator H. However, an alternative is to use the partial energy quantities. Then, the partial power balances for separate incident energies and reflected energies can be written as

$$\frac{dP_l^+}{ds} + (\eta\omega + a_l) W_l^+ = 0 \quad \text{and} \quad \frac{dP_l^-}{ds} + (\eta\omega + a_l) W_l^- = 0. \tag{14}$$

Obviously, the global power balance given in expression (13) can be deduced by summing these relationships. In addition, using the partial quantities, the relationships between the partial energy density and active energy flow are merely a proportionality. Then

$$P_l^+ = c_g^l W_l^+ \quad \text{and} \quad P_l^- = -c_g^l W_l^-, \tag{15}$$

where c_g^l is the group velocity associated to the longitudinal wave.

The group velocity is the speed at which energy flows. Its definition in terms of the longitudinal wave number is

$$c_g^l = \frac{d\omega}{dk_l}. \tag{16}$$

Alternatively, its value can be evaluated directly from the proportionality constants given in Appendix B.

The partial constitutive laws given in Eq. (15) are established for a nondissipative wave guide[12] since the employed group velocity is that for an undamped system. For SEF developments, the damping loss factor is assumed to be very small (first assumption), and then relationships (15) are assumed to remain valid. In addition, the effects of damping are taken into account by way of the power being dissipated in the power balance relations (14).

Substracting the relationships (14) yields

$$\frac{d}{ds}(P_l^+ - P_l^-) + (\eta\omega + a_l)(W_l^+ - W_l^-) = 0.$$

Using proportionality relationships (15)

$$c_g^l \frac{d}{ds}(W_l^+ + W_l^-) + \frac{\eta\omega + a_l}{c_g^l}(P_l^+ + P_l^-) = 0.$$

Thus by virtue of (12), the global active energy flow, P_l, is simply proportional to the first derivative of the global energy density W_l:

$$P_l = -\frac{c_g^{l^2}}{\eta\omega + a_l}\frac{dW_l}{ds}. \tag{17}$$

Finally, combining expressions (17) and (13), one obtains the explicit energy equation for tangential movement of curved waveguide:

$$\frac{d^2W_l}{ds^2} - \frac{(\eta\omega + a_l)^2}{c_g^{l^2}} W_l = 0. \tag{18}$$

Let us define the real wave number k_∞^l as the wave number of the straight longitudinal excited nondissipative system: $k_\infty^l \overset{\text{def}}{=} \omega\sqrt{\rho/E_0}$. Then, when the nondimensional quantity Rk_∞^l becomes infinite $Rk_\infty^l \to \infty$, the group velocity c_g^l is the same as for straight bar, ω/k_∞^l, and the exchanged coefficient a_l vanishes, so energy equation (18) is the same as that developed in Refs. 8 and 13:

$$\frac{d^2W}{ds^2} - \eta^2 k_\infty^l W = 0. \tag{19}$$

The solution of Eq. (18) is the sum of an incident and a reflected term:

$$W_l(s) = A^+ e^{[(\eta\omega + a_l)/c_g^l]s} + A^- e^{[(\eta\omega + a_l)/c_g^l]s}. \tag{20}$$

To solve this problem completely, one must determine the energy amplitudes A^+ and A^- occurring in the previous expression (20). To calculate the energy magnitudes A^+ and A^-, the classical boundary conditions may be written in terms of the variables W_l and P_l. A complete study concerning the energetic boundary and coupling conditions has been already made[14] in the case of a simple Euler–Bernoulli beam and other waveguides.[15] The general procedure proposed there remains, of course, valid in the case of radial waves in the waveguide. For instance, at an excited node located at s_0, the active energy flow is assumed to be known.

$$P_l(s_0) = P_{inj}. \tag{21}$$

For a dissipative end located at s_1, the equivalent energy boundary condition is

$$P_l^-(s_1) = r_l P_l^+(s_1)$$

or

$$(P_l - c_g^l W_l)(s_0) = r_l (P_l + c_g^l W_l)(s_0), \tag{22}$$

where r_l is a reflection coefficient. Note that this coefficient may be smaller than one even for a nondissipative end due to mode conversion: A part of longitudinal incident energy flow is converted into flexural energy flow.

Boundary conditions (21) and (22), when combining with relationship (20), allow the energy density magnitude A^+ and A^- to be calculated.

B. The envelope energy expression

Energy equation (18) given above allows the prediction of the level of the total energy density, and the active energy flow without interferences. Its solution (20) has a smooth spatial variation with no local oscillations. In this section, further information is deduced from the energy equation (18) by comparing it to the solution of the equations of motion (4).

Indeed, the particular solution of Eqs. (4), corresponding to a couple of longitudinal waves, can be written

$$\begin{aligned} u &= a^+ e^{-ik_l s} + a^- e^{ik_l s}, \\ \nu &= b^+ e^{-ik_l s} + b^- e^{ik_l s}. \end{aligned} \tag{23}$$

By virtue of (6), a proportionality exists between $b^\pm$ and $a^\pm$. Let ξ_l denote this proportionality, so that $b^+ = \xi_l a^+$ and $b^- = -\xi_l a^-$ where

$$\xi_l = \frac{\omega^2 R^2/c_0^2 - k_l^2 R^2 - k_l^2\mu^2}{i(k_l R + k_l^3 R\mu^2)} = \frac{-i(k_l R + k_l^3 R\mu^2)}{\omega^2 R^2/c_0^2 - 1 - k_l^4 R^2\mu^2}. \tag{24}$$

By introducing expression (23) in the longitudinal energy density expression given by (10), the following formulas for the total energy density are obtained:

$$\begin{aligned} W_l(s) &= W_{\text{smooth}}(s) + W_{\text{asc}}(s), \\ W_{\text{smooth}}(s) &= \frac{1}{4}\left[\rho S\omega^2 + E_0 S\left|\frac{\xi_l}{R} - ik_l\right|^2\right] \\ &\quad \times (|a^+|^2 e^{2\,\text{Imag}(k_l)s} + |a^-|^2 e^{-2\,\text{Imag}(k_l)s}), \\ W_{\text{asc}}(s) &= \frac{1}{4}\left[\rho S\omega^2 - E_0 S\left|\frac{\xi_l}{R} - ik_l\right|^2\right] \\ &\quad \times (a^+ a^{-*} e^{-2i\,\text{Real}(k_l)s} + a^- a^{+*} e^{2i\,\text{Real}(k_l)s}). \end{aligned} \tag{25}$$

The comparison between the total energy density (25) calculated using solution (23) and the one given in expression (20) and evaluated from the smooth energy formulation, shows that relationship (20) is the smooth term that occurs in (25). This first term, corresponding to the real exponential terms, has a slow spatial variation, while the second energy term has an oscillating spatial variation. In addition, a mere identification gives the magnitudes A^+ and A^- in terms of $|a^+|^2$ and $|a^-|^2$:

$$\begin{aligned} A^+ &= \frac{1}{4}\left[\rho S\omega^2 + E_0 S\left|\frac{\xi_l}{R} - ik_l\right|^2\right]|a^+|^2, \\ A^- &= \frac{1}{4}\left[\rho S\omega^2 + E_0 S\left|\frac{\xi_l}{R} - ik_l\right|^2\right]|a^-|^2. \end{aligned} \tag{26}$$

Moreover, the magnitude of the oscillating components W_{osc} is given by

$$\begin{aligned} M_{\text{asc}} &= \frac{1}{2}\left|\rho S\omega^2 - E_0 S\left|\frac{\xi_l}{R} - ik_l\right|^2\right||a^- a^{+*}| \\ &= 2\frac{\left|\rho S\omega^2 - E_0 S\left|\frac{\xi_l}{R} - ik_l\right|^2\right|}{\left|\rho S\omega^2 + E_0 S\left|\frac{\xi_l}{R} - ik_l\right|^2\right|}\sqrt{A^- A^+}, \end{aligned} \tag{27}$$

where A^+ and A^- are the energy magnitudes predicted by SEF.

In the case of large value of Rk_∞^l, the magnitude of the oscillating components is simply

$$M_{\text{asc}} \approx 2\sqrt{AB}/R^2 k_\infty^{l^2}. \tag{28}$$

As a result of this remark, the energy equation (20) contains additional information on the lower and the upper energy envelopes:

$$W_{\text{upper}}(s)=A^{+}e^{[(\eta\omega+a_l)/c_g^l]s}+A^{-}e^{[(\eta\omega+a_1)/c_g^l]s}+M_{\text{asc}},$$
$$W_{\text{lower}}(s)=A^{+}e^{[(\eta\omega+a_l)/c_g^l]s}+A^{-}e^{[(\eta\omega+a_l)/c_g^l]s}-M_{\text{asc}}. \tag{29}$$

Consequently, SEF for tangential waves predicts not only the smooth level of the total energy density and active energy flow, but their upper and lower envelopes too.

IV. ENERGY MODEL FOR RADIAL WAVES

In this section an energy model for a system containing only radial waves is developed in a similar way as for the system with only tangential waves in Sec. III.

A. Energy equation

Let us consider the solution of the frequency equation. In Eq. (8) we noted that two kinds of wave numbers exist for radial case: an evanescent wave number k_f^e and a propagating wave number k_f^p. The amplitudes of the evanescent waves decrease rapidly away from boundaries, and are then neglected for SEF developments (second assumption). Therefore the only group velocity to be considered for radial waves is associated to the wave number for propagating waves:

$$c_g^f=\frac{d\omega}{dk_f^p}. \tag{30}$$

Hence, the problem associated with the propagating radial waves becomes similar to the tangential case treated before. In particular, the relationship between the global active energy flow and total energy density is as follows:

$$P_f=-\frac{c_g^{f^2}}{\eta\omega+a_f}\frac{dW_f}{ds}. \tag{31}$$

By introducing this constitutive law in the active power balance, one obtains the following energy equation for the radial behavior of a curved waveguide:

$$\frac{d^2W_f}{ds^2}-\frac{(\eta\omega+a_f)^2}{c_g^{f^2}}W_f=0. \tag{32}$$

By introducing the wave number k_∞^f corresponding to a straight nondissipative Euler–Bernoulli beam, $k_\infty^f \underset{\text{def}}{=}(\rho S\omega^2/E_0I)^{1/4}$, and by assuming the quantity Rk_∞^f to be very large, the energy equation obtained is merely the well-known energy equation developed by Refs. 7, 8, and 13:

$$\frac{d^2W}{ds^2}-\frac{\eta^2k_\infty^{f^2}}{4}W=0. \tag{33}$$

The solution of energy equation (32) is

$$W_f(s)=A^{+}e^{-[(\eta\omega+a)/c_g^f]s}+A^{-[(\eta\omega+a)/c_g^f]s}. \tag{34}$$

The equation above is solved using energetic boundary conditions. Here, relationships similar to (21) and (22) given in the tangential case are valid.

B. The energy envelope expression

In a manner similar to that used for tangential waves, the upper and lower total energy density envelopes can be determined. Let us consider a couple of propagating flexural waves where the resulting tangential and radial displacements are as follows:

$$u=a^{+}e^{-ik_f^ps}+a^{-}e^{ik_f^ps},$$
$$\nu=b^{+}e^{-ik_f^ps}+b^{-}e^{ik_f^ps}. \tag{35}$$

The proportionality between $b^{\pm}$ and $a^{\pm}$ still applies i.e., $b^{+}=\xi_f a^{+}$ and $b^{-}=-\xi_f a^{-}$ where

$$\xi_f=\frac{\omega^2R^2/c_0^2-k_f^{p^2}R^2-k_f^{p^2}\mu^2}{i(k_f^pR+k_f^{p^3}R\mu^2)}$$
$$=\frac{-i(k_f^pR+k_f^{p^3}R\mu^2)}{\omega^2R^2/c_0^2-1-k_f^{p^4}R^2\mu^2}. \tag{36}$$

Then, the expression for the transverse energy density in case of a flexural propagating wave is:

$$W_f(s)=W_{\text{smooth}}(s)+W_{\text{asc}}(s),$$
$$W_{\text{smooth}}(s)=\frac{1}{4}\left[\rho S\omega^2|\xi_f|^2+E_0I\left|\frac{ik_f^p}{R}-k_f^{p^2}\xi_f\right|^2\right]$$
$$\times(|a^{+}|^2e^{2\,\text{Imag}(k_f^p)s}+|a^{-}|^2e^{-2\,\text{Imag}(k_f^p)s}),$$
$$W_{\text{asc}}(s)=\frac{-1}{4}\left[\rho S\omega^2|\xi_f|^2+E_0I\left|\frac{ik_f^p}{R}-k_f^{p^2}\xi_f\right|^2\right]$$
$$\times(a^{+}a^{-*}e^{-2i\,\text{Real}(k_f^p)s}+a^{-}a^{+*}e^{2\,\text{Real}(k_f^p)s}). \tag{37}$$

Hence, as in the tangential case, the magnitude of the oscillating field is given by

$$M_{\text{asc}}=2\sqrt{A^{+}A^{-}}. \tag{38}$$

It is surprising that this magnitude does not depend explicitly on the presence of curvature. In fact, the obtained magnitude of oscillations $2\sqrt{A^{+}A^{-}}$ is exactly the one given in Ref. 16 for the case of a straight Euler–Bernoulli beam. Obviously, the curvature affects the values of the coefficients A^{+} and A^{-} by means of the group velocity which depends on this curvature.

In the case of radial waves in curved wave guides, the upper and lower total energy density variation are given simply by

$$W_{\text{upper}}(s)=A^{+}e^{[(\eta\omega+a_f)/c_g^f]s}+A^{-}e^{[(\eta\omega+a_f)/c_g^f]s}+M_{\text{asc}},$$
$$W_{\text{lower}}(s)=A^{+}e^{[(\eta\omega+a_f)/c_g^f]s}+A^{-}e^{[(\eta\omega+a_f)/c_g^f]s}-M_{\text{asc}}. \tag{39}$$

V. COMPLETE ENERGY MODEL OF CURVED BEAMS

The case of the simultaneous propagation of radial and tangential waves in the waveguide is more complicated than the propagation of the individual waves. Every kind of energy quantity which was previously defined in Sec. I, appears simultaneously in this case:

$$P_l^+, P_l^-, P_f^+, P_f^-, W_l^+, W_l^-, W_f^+, W_f^- . \tag{40}$$

To these quantities, we add the active energy flow, which characterizes the exchange between the longitudinal (tangential waves) and the flexural (radial waves) behavior. The exchanged energy flows are

$$p_{lf}^+, p_{lf}^- . \tag{41}$$

Let us generalize the derivation of the energy equations established for a single wave. We noted that when interferences were neglected, a linear superposition principle is valid for energy quantities. Relationship (12) then becomes

$$Z = Z^+ + Z^- \quad \text{with} \quad Z = P, \ W, \ \text{or} \ p. \tag{42}$$

In this case, the local power balance is composed of two coupled equations due to the presence of the exchanged energy flows:

$$\begin{aligned} &\frac{d}{ds}\begin{pmatrix} P_l^+ \\ P_f^+ \end{pmatrix} + \begin{pmatrix} p_{\text{diss}}^{l+} \\ p_{\text{diss}}^{f+} \end{pmatrix} + \begin{pmatrix} p_{lf}^+ \\ -p_{lf}^+ \end{pmatrix} = \begin{pmatrix} 0 \\ 0 \end{pmatrix}, \\ &\frac{d}{ds}\begin{pmatrix} P_l^- \\ P_f^- \end{pmatrix} + \begin{pmatrix} p_{\text{diss}}^{l-} \\ p_{\text{diss}}^{f-} \end{pmatrix} + \begin{pmatrix} p_{lf}^- \\ -p_{lf}^- \end{pmatrix} = \begin{pmatrix} 0 \\ 0 \end{pmatrix}. \end{aligned} \tag{43}$$

The damping model, $p_{\text{diss}} = \eta\omega W$ is still valid. Now, the constitutive relationships between the propagating quantities have to be established. In the coupled case, relationships (15) used for both radial waves and tangential waves are still valid, but the proportionality coefficient becomes a 2 by 2 matrix:

$$\begin{pmatrix} P_l^+ \\ P_f^+ \end{pmatrix} = [C_g]_{2\times 2}\begin{pmatrix} W_l^+ \\ W_f^+ \end{pmatrix}, \quad \begin{pmatrix} P_l^- \\ P_f^- \end{pmatrix} = -[C_g]_{2\times 2}\begin{pmatrix} W_l^- \\ W_f^- \end{pmatrix}. \tag{44}$$

An additional relationship is written for the exchanged energy flows as follows:

$$\begin{pmatrix} p_{lf}^+ \\ -p_{lf}^+ \end{pmatrix} = [A]_{2\times 2}\begin{pmatrix} W_l^+ \\ W_f^+ \end{pmatrix}, \quad \begin{pmatrix} p_{lf}^- \\ -p_{lf}^- \end{pmatrix} = [A]_{2\times 2}\begin{pmatrix} W_l^- \\ W_f^- \end{pmatrix}, \tag{45}$$

where $[A]$ is a 2 by 2 matrix with a second row equal to the opposite of the first:

$$[A] = \begin{pmatrix} \lambda & \gamma \\ -\lambda & -\gamma \end{pmatrix}.$$

Note that the matrix appearing in the second relationship (45) is not the opposite of those in the first relationship contrary to Eq. (44). This means that when the propagation direction of a wave is inverted, there is no modification of the active energy flow exchanged between the radial and tangential waves. The complete expressions of the matrices $[C_g]$ and $[A]$ are given in the Appendix B.

Given the constitutive relationships in Eqs. (44) and (45), it becomes easy to deduce the equation for the energy flow for coupled radial and tangential waves. The sum of expressions (43) leads to the global power balance:

$$\frac{d}{ds}\begin{pmatrix} P_l \\ P_f \end{pmatrix} + \eta\omega\begin{pmatrix} W_l \\ W_f \end{pmatrix} + [A]_{2\times 2}\begin{pmatrix} W_l \\ W_f \end{pmatrix} = \begin{pmatrix} 0 \\ 0 \end{pmatrix}. \tag{46}$$

The difference between the expressions yields the constitutive relation between the global energetic variables:

$$\begin{aligned} &\frac{d}{ds}\left\{\begin{pmatrix} P_l^+ \\ P_f^+ \end{pmatrix} - \begin{pmatrix} P_l^- \\ P_f^- \end{pmatrix}\right\} + (\eta\omega[I]_{2\times 2} + [A]_{2\times 2}) \\ &\times\left\{\begin{pmatrix} W_l^+ \\ W_f^+ \end{pmatrix} - \begin{pmatrix} W_l^- \\ W_f^- \end{pmatrix}\right\} = \begin{pmatrix} 0 \\ 0 \end{pmatrix}, \end{aligned} \tag{47}$$

where $[I]$ is the identity matrix. Substituting (44) for each term yields

$$\begin{pmatrix} P_l \\ P_f \end{pmatrix} = -[C_g](\eta\omega[I] + [A])^{(-1)}[C_g]\frac{d}{ds}\begin{pmatrix} W_l \\ W_f \end{pmatrix}. \tag{48}$$

Thus by substituting expressions (48) into (46), the system of energy equations for the coupled problem is written as

$$\frac{d^2}{ds^2}\begin{pmatrix} W_l \\ W_f \end{pmatrix} - ([C_g]^{(-1)}(\eta\omega[I] + [A]))^2\begin{pmatrix} W_l \\ W_f \end{pmatrix} = \begin{pmatrix} 0 \\ 0 \end{pmatrix}. \tag{49}$$

The solutions of this system introduce four energy magnitudes which may be evaluated from energy boundary conditions. For instance, at an excited node, the injected active energy flow is assumed to be known, and then

$$\begin{pmatrix} P_l \\ P_f \end{pmatrix}(s_0) = \begin{pmatrix} P_{l_{\text{inj}}} \\ P_{f_{\text{inj}}} \end{pmatrix}. \tag{50}$$

Moreover, at a dissipative end, the following relationship is written:

$$\begin{pmatrix} P_l^- \\ P_f^- \end{pmatrix}(s_1) = [R]_{2\times 2}\begin{pmatrix} P_l^+ \\ P_f^+ \end{pmatrix}(s_1)$$

or (51)

$$\begin{aligned} &\left[\begin{pmatrix} P_l \\ P_f \end{pmatrix} - [C_g]_{2\times 2}\begin{pmatrix} W_l \\ W_f \end{pmatrix}\right](s_1) \\ &= [R]_{2\times 2}\left[\begin{pmatrix} P_l \\ P_f \end{pmatrix} + [C_g]_{2\times 2}\begin{pmatrix} W_l \\ W_f \end{pmatrix}\right](s_1). \end{aligned}$$

The matrix $[R]$ is constituted from four reflection coefficients which illustrate mode-conversion phenomena. Each coefficient has a non-negative value smaller than one. The nondissipative condition leads to special relationships: The sum of each column must be equal to one.

VI. NUMERICAL SIMULATIONS

Consider a curved beam with mass density $\rho = 7800\ \text{kg/m}^3$, Young modulus $E = 2.1\ e^{11}\ \text{N/m}^2$, inertia $I = 8.3\ e^{-10}\ \text{m}^4$, cross section $S = 1\ e^{-4}\ \text{m}^2$, length $L = 1\ \text{m}$, and radius of curvature $R = 0.25\ \text{m}$. The damping ratio η is taken to be equal to 0.05.

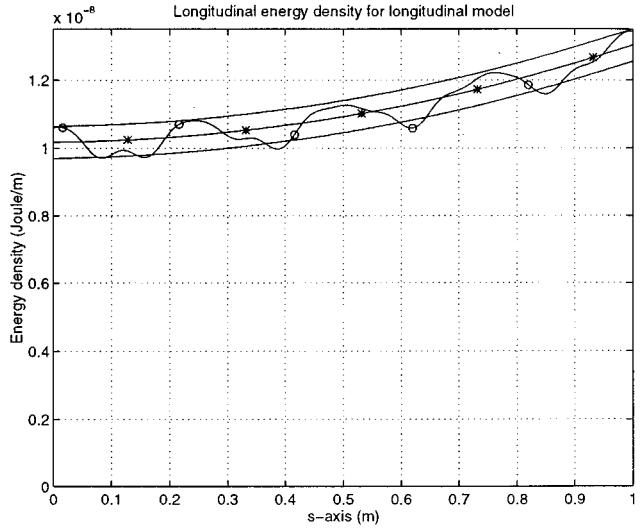

FIG. 5. Longitudinal energy density variation versus s axis; ○ equation of motion (4); * energetic equation (18) and its associated upper and lower bounds given in (29).

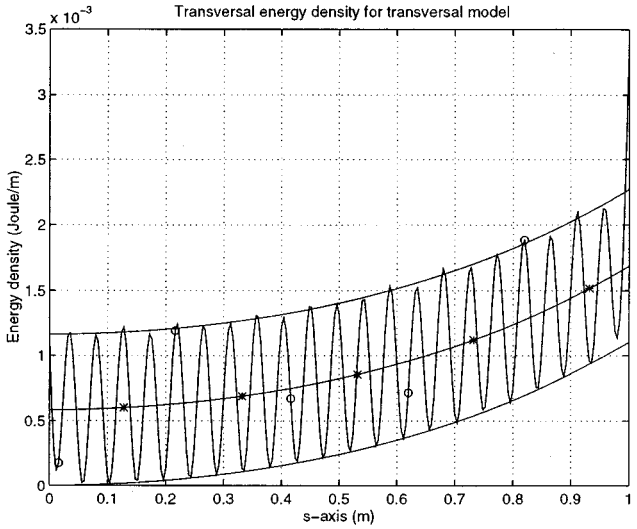

FIG. 7. Transverse energy density variation versus s axis; ○ equation of motion (4); * energetic solution (34) and its associated upper and lower bounds given in (39).

First of all, the curved beam is excited at its right end node 1 by a longitudinal force of strength 1 N. Following (21), the longitudinal active energy flow P_l is assumed to be known at node 1. At the left end of the waveguide, node 0, the clamped end boundary condition is used which corresponds to the relationship (22) with an appropriate reflection coefficient (see Appendix C). Two calculations are performed. The first solves governing equations (4) and the longitudinal energy density and energy flow are then evaluated using Eqs. (10) and (11). This classical calculation is taken as a reference. On the other hand, combining expressions (21) and (22), one can find the energy magnitudes A^+ and A^- and then the energy quantities are obtained from Eqs. (17) and (20). This is the SEF result. The results of the simulations are given in Figs. 5 and 6 for a pure-tone excitation at $f=11\,000$ Hz. Thus it can be shown that the energy model (20) produces a prediction of the local space average of total energy density and active energy flow. Therefore, as the solution given by this model varies slowly in space, a numerical implementation of this procedure with finite elements for instance, would require a few degrees of freedom. This is very attractive in the mid- and high-frequency domain. Finally, note that the energy flow predicted by SEF does not vanish at the clamped end. Actually, the local energy flow predicted by the equation of motion will disappear but its mean value over a vicinity will not disappear. This apparent dissipation is relevant to mode conversion phenomena.

Second, the curved beam is excited at node 1 by a transverse force strength 1 N. The injected active energy flow is assumed to be known at this node. At the end of this waveguide the energetic clamped end (22) is still valid at this stage. The energy system to be solved in order to determine the energy magnitudes A^+ and A^- is formally the same as in the longitudinal case. Results are given in Figs. 7 and 8. The

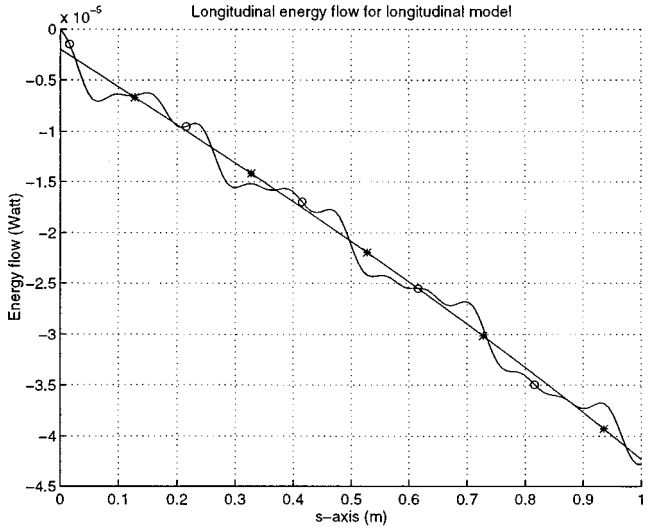

FIG. 6. Longitudinal energy flow variation versus s axis; ○ equation of motion (4); * energetic equation (18).

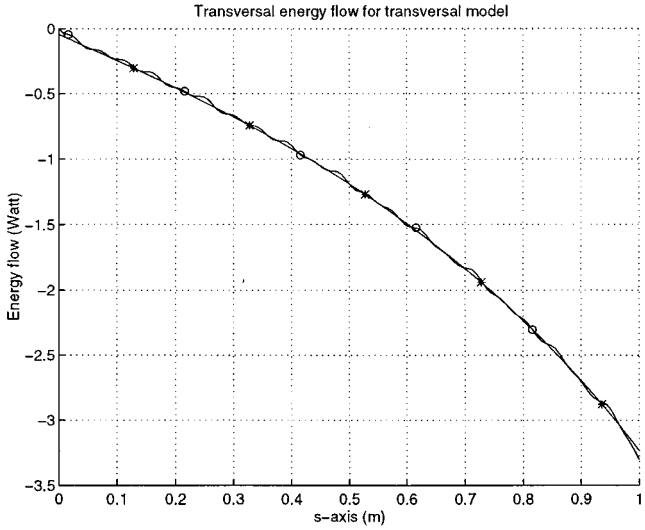

FIG. 8. Transverse energy flow variation versus s axis; ○ equation of motion (4); * energetic solution (34).

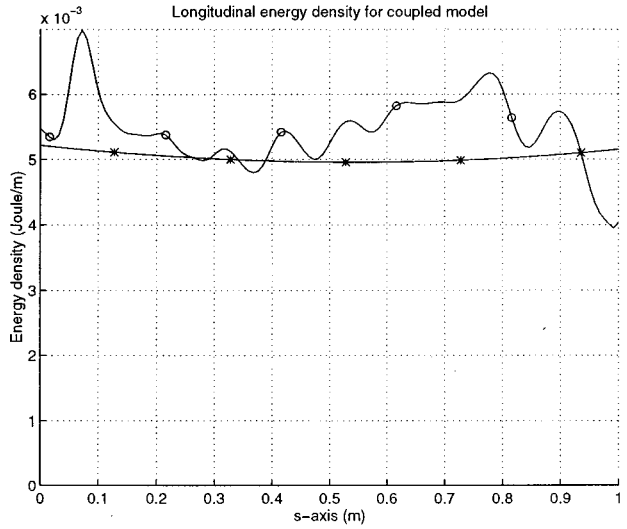

FIG. 9. Longitudinal energy density variation versus s axis; ○ equation of motion (4); * energetic equation (49).

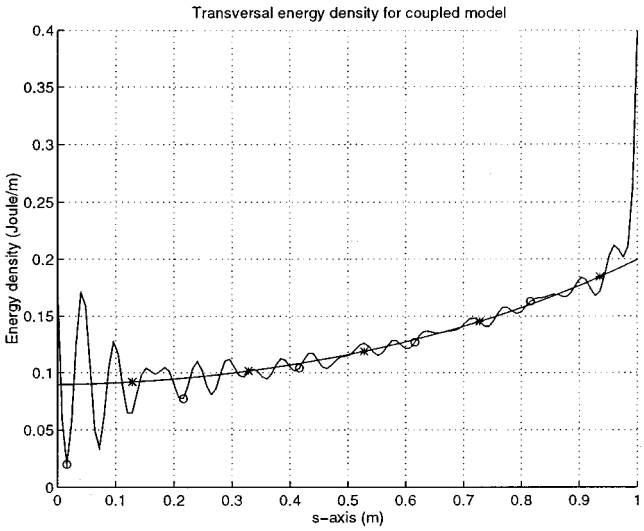

FIG. 11. Transverse energy density variation versus s axis; ○ equation of motion (4); * energetic equation (49).

comparison between the classic calculation of the energy density and the energy flow from the kinematic model (4) shows that SEF again allows the prediction of the required smooth level of the energy density and the energy flow. Moreover, the application of relationships (39) permits the upper and lower energy envelopes to be known.

Finally, the complete coupled system is simulated. Two forces are applied: a longitudinal force of strength 5 N and an antiphase transverse force of strength 1 N. The results of a simulation are given in Figs. 9–12 versus the curvilinear coordinate s. However, in opposition to previous simulations where the excitation was in pure tone, the classical calculation is now performed over the octave 5000 Hz–10 000 Hz. Actually, the matrix $[R]$ has been determined for a semi-infinite system and then it is applicable to a finite system in a frequency-average sense. However, it turns out that the differences between the pure-tone reflection coefficients (not determined here) and the semi-infinite ones are small. Then, as long as we are interested in just one kind of energy induced by respective load, a pure-tone simulation is satisfactory. But, for the coupled model, due to the large domination of longitudinal energy level by transverse energy level, a small miscalculation of the transverse reflection coefficient may induce a large difference on longitudinal energy level. This is why frequency averages are needed. Results given in Figs. 9–12 are the average over this octave. The energetic calculation stems from (49) with boundary conditions (50) and (51). However, the injected power appearing in (50) is not the exact pure-tone value at the mean frequency but the mean value for this octave. The latter is obtained by considering the infinite impedance: The injected power is the one created by the same excitation applied to the equivalent infinite curved beam. Note that the energy flows do not vanish at the clamped end as previously observed. The longitudinal energy flow at the clamped end is exactly the opposite of the

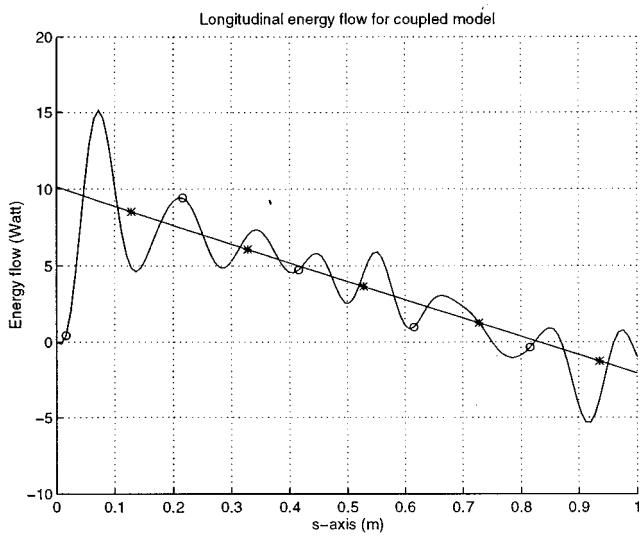

FIG. 10. Longitudinal energy flow variation versus s axis; ○ equation of motion (4); * energetic equation (49).

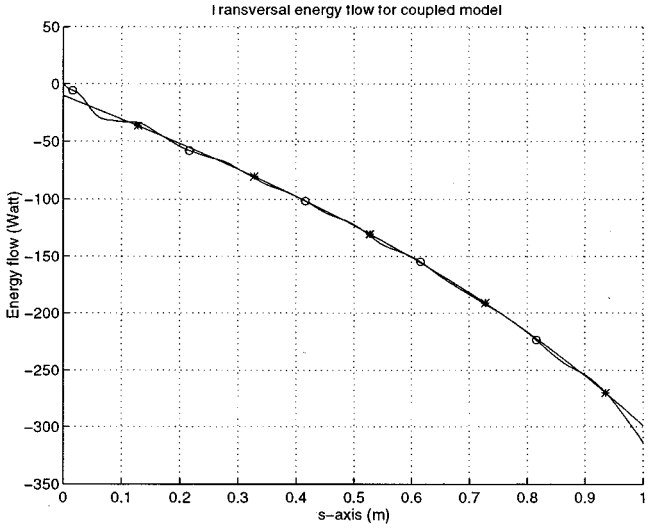

FIG. 12. Transverse energy flow variation versus s axis; ○ equation of motion (4); * energetic equation (49).

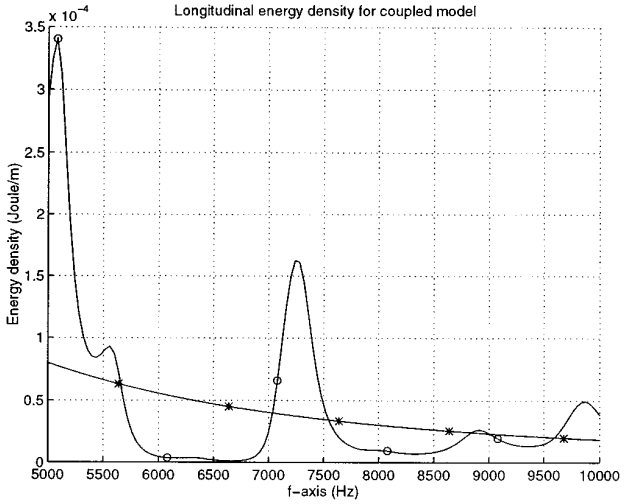

FIG. 13. Longitudinal energy density variation versus f axis; ○ equation of motion (4); * energetic equation (49).

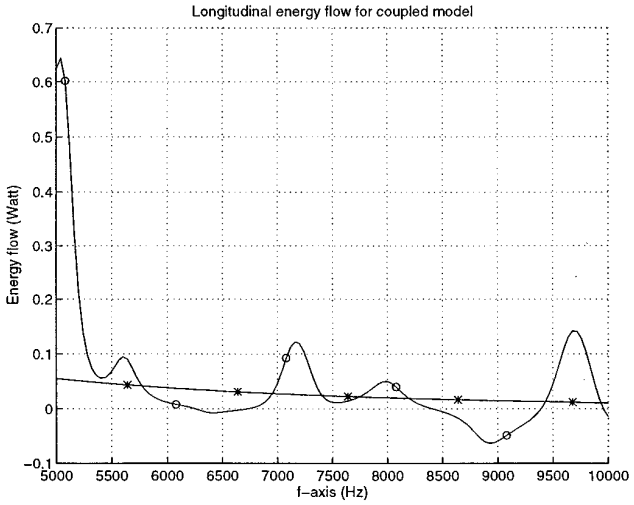

FIG. 14. Longitudinal energy flow variation versus f axis; ○ equation of motion (4); * energetic equation (49).

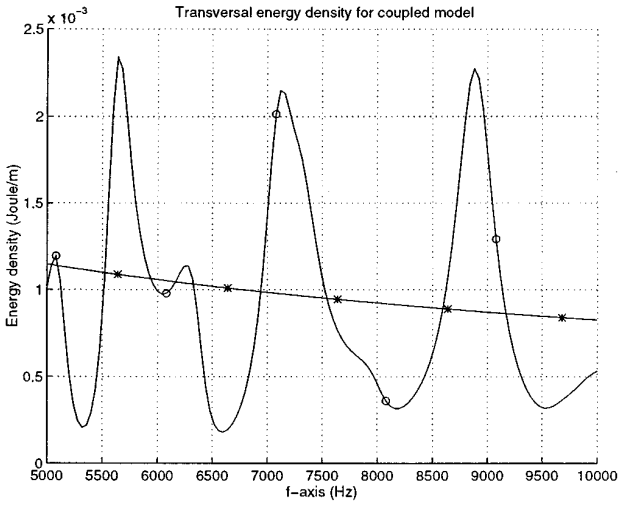

FIG. 15. Transverse energy density variation versus f axis; ○ equation of motion (4); * energetic equation (49).

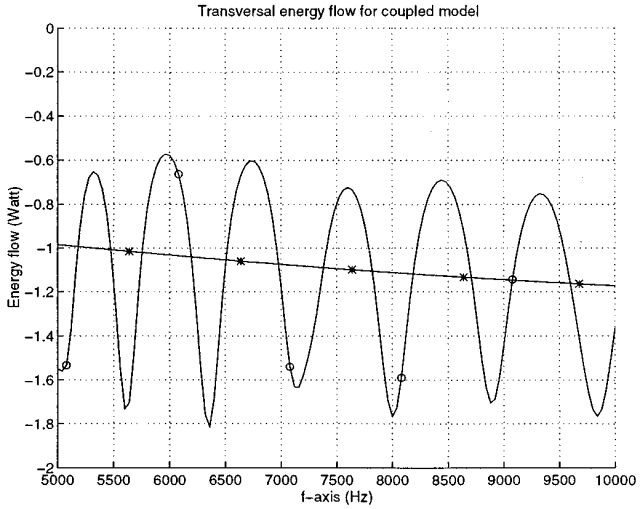

FIG. 16. Transverse energy flow variation versus f axis; ○ equation of motion (4); * energetic equation (49).

transverse energy flow at the same point. So, the clamped end is a nondissipative end. In Figs. 13–16 the energy quantities are plotted at a point versus frequency. It can be observed that the energy quantities issued from SEF are not only the local space average of exact quantities but also the frequency average. This average must be performed over a frequency band which contains at least several eigenfrequencies.

VII. CONCLUDING REMARKS

In this paper, a new formulation has been proposed to allow the prediction of the dynamical behaviour of curved beams at high frequencies. This formulation is based on a solely energetic variables which are the total energy density and the active energy flow. The results given here generalize those given in the case of straight rods and beams.[7,8,13] This method is numerically attractive in the mid- and high-frequency range.

Three models have been studied. The first one is concerned only with the longitudinal behavior. Then by considering a longitudinal wave alone, this model allows the prediction of the smooth part of the longitudinal energy density and energy flow. A similar model has been developed for the flexural behavior. However an additional assumption is required: The evanescent wave has to be neglected. In these two models, the upper and lower envelops of the energy density have been also evaluated. Finally, a complete model including the effect of the exchanged energy flow between longitudinal and flexural behavior, has been proposed.

ACKNOWLEDGMENTS

The authors gratefully acknowledge E. Luzzato (EDF–DER Département d'Acoustique et de Mécanique Vibratoire), and R. Aquilina (Centre d'Étude et de Recherche de la Discrétion Acoustique des Navires) for their kind help and advices, and R. Lambrech for editing this manuscript.

APPENDIX A

Let us rewrite frequency equation (7) by using the nondimensional quantities $\overline{k}=k\mu$, $\overline{\omega}=\mu\omega/c_0$, and $\overline{\epsilon}=\mu/R$:

$$\overline{k}^6-(\overline{\omega}^2+2\overline{\epsilon}^2)\overline{k}^4+(\overline{\epsilon}^4-\overline{\omega}^2(1+\overline{\epsilon}^2))\overline{k}^2+\overline{\omega}^2(\overline{\omega}^2-\overline{\epsilon}^2)=0. \tag{A1}$$

This is a bicubic equation for the unknown $\overline{k}$. As the wave number for a straight rod is $k_\infty^l=\omega/c_0$, the solution $\overline{k}^l$ of Eq. (A1) associated with longitudinal waves must tend to $\overline{\omega}$ as the small parameter $\overline{\epsilon}$ tends to zero. Moreover the value of $\overline{k}^l$ cannot depend on the sign of the radius of curvature R. Then, an asymptotic expression of $\overline{k}^l$ must take the form

$$\overline{k}^l=\overline{\omega}+a\overline{\epsilon}^2+o(\overline{\epsilon}^2). \tag{A2}$$

Substituting (A2) in (A1) yields

$$\overline{k}^l=\overline{\omega}+\frac{1+3\overline{\omega}^2}{2\overline{\omega}(\overline{\omega}^2-1)}\,\overline{\epsilon}^2+o(\overline{\epsilon}^2). \tag{A3}$$

An analogous calculation for the transverse wave number leads to

$$\overline{k}_f^p=\sqrt{\overline{\omega}}+\frac{3+\overline{\omega}}{4\sqrt{\overline{\omega}}(1-\overline{\omega})}\,\overline{\epsilon}^2+o(\overline{\epsilon}^2). \tag{A4}$$

These relationships are valid in case of large radius of curvature.

APPENDIX B

Let us consider a harmonic wave of form (5). The admissible values for the parameter k are given by dispersion equation (7). In order to simplify the following relationships, we note k_1 (resp. k_2), the incident longitudinal wave number k_1 (resp. the incident propagating flexural wave number k_f^p).

Moreover, referring to (6), for each harmonic wave of form (5), the corresponding displacement magnitudes a and b are proportional. So, let ξ_i designate the ratio of the displacement amplitudes b_i/a_i for $i=1,2$. The expressions for ξ_i are respectively given in Eqs. (36) and (24).

Now, let us assume that an incident radial wave and an incident tangential wave occur simultaneously in a given system. The total displacements are

$$u=a_1e^{-ik_1s}+a_2e^{-ik_2s} \quad \text{and} \quad \nu=b_1e^{-ik_1s}+b_2e^{-ik_2s}. \tag{B1}$$

Then substituting (B1) into energy expressions (10) and (11), and neglecting the cross product terms which are due to interferences between radial and tangential waves, leads to

$$W_l^+=\sum_{i=1}^{2}\frac{1}{4}\left\{\rho S\omega^2+\frac{E_0S}{R^2}\,|\xi_i-ik_iR|^2\right\}\times[|a_i|^2e^{2\,\mathrm{Imag}(k_i)s}],$$

$$W_f^+=\sum_{i=1}^{2}\frac{1}{4}\left\{\rho S\omega^2|\xi_i|^2+\frac{E_0I}{R^2}\,|k_i|^2|1+ik_i\xi_iR|^2\right\}\times[|a_i|^2e^{2\,\mathrm{Imag}(k_i)s}],$$

$$P_l^+=\sum_{i=1}^{2}\mathrm{Real}\left\{\frac{i\omega}{2}\left[\frac{ES}{R}\,(\xi_i-ik_iR)-\frac{EI}{R^2}\,ik_i(1+ik_i\xi_iR)\right]\right\}[|a_i|^2e^{2\,\mathrm{Imag}(k_i)s}], \tag{B2}$$

$$P_f^+=\sum_{i=1}^{2}\mathrm{Real}\left\{\frac{i\omega}{2}\,\frac{EI}{R}\,[-k_i^2(1+ik_i\xi_iR)\xi_i^*-|k_i|^2(1+ik_i\xi_iR)\xi_i^*]\right\}[|a_i|^2e^{2\,\mathrm{Imag}(k_i)s}],$$

$$p_{lf}^+=\sum_{i=1}^{2}\mathrm{Real}\left\{\frac{i\omega}{2}\,\frac{1}{R^2}\,[ES(\xi_i-ik_iR)\xi_i^*-EI|k_i|^2(1+ik_i\xi_iR)]\right\}[|a_i|^2e^{2\,\mathrm{Imag}(k_i)s}].$$

The corresponding quantities with a minus superscript are obtained by substituting $-k_i$ and $-\xi_i$ everywhere. Relationships (B2) can be written in a simple matrix form as

$$\begin{pmatrix}W_l^+\\W_f^+\end{pmatrix}=[w]_{2\times2}\begin{pmatrix}|a_1|^2e^{2\,\mathrm{Imag}(k_1)s}\\|a_2|^2e^{2\,\mathrm{Imag}(k_2)s}\end{pmatrix}\begin{pmatrix}P_l^+\\P_f^+\end{pmatrix}=[\wp]_{2\times2}\begin{pmatrix}|a_1|^2e^{2\,\mathrm{Imag}(k_1)s}\\|a_2|^2e^{2\,\mathrm{Imag}(k_2)s}\end{pmatrix}p_{lf}^+=[p]_{1\times2}\begin{pmatrix}|a_1|^2e^{2\,\mathrm{Imag}(k_1)s}\\|a_2|^2e^{2\,\mathrm{Imag}(k_2)s}\end{pmatrix}. \tag{B3}$$

The coefficients of the matrix $[w]_{2\times2}$, $[\wp]_{2\times2}$, and $[p]_{1\times2}$ are easily identified from expressions (B2). Thus the matrix $[C_g]_{2\times2}$ and $[A]_{2\times2}$ are given by

$$[C_g]=[\wp][w]^{(-1)} \quad \text{and} \quad [\lambda\ \gamma]=[p][w]^{(-1)}. \tag{B4}$$

When either the longitudinal or transverse model is considered, the group velocity and the coefficients a_l and a_f are determined from these matrices:

$$c_g^l=C_{g_{1,1}} \quad \text{and} \quad c_g^f=C_{g_{2,2}},\qquad a_l=\lambda \quad \text{and} \quad a_f=-\mu. \tag{B5}$$

APPENDIX C

Let us determine the reflection coefficients matrix occurring in (51). For this purpose, an incident longitudinal wave of form (5) whose magnitudes are denoted by a_l^+ and b_l^+ is considered first. When this wave encounters the clamped end, some reflected longitudinal, propagating transverse and evanescent transverse waves are created. Their magnitudes are denoted, respectively, a_l^-, b_l^-, $a_f^{p^-}$, $b_f^{p^-}$, $a_f^{e^-}$, and $b_f^{e^-}$. By applying the classical clamped boundary conditions (i.e., $\mu=\nu=\theta=0$) and recalling that magnitudes b are proportional to magnitudes a, three equations determine the magnitudes a_l^-, $a_f^{p^-}$, $a_f^{e^-}$ in terms of a_l^+;

$$\begin{pmatrix}a_l^-\\a_f^{p^-}\\a_f^{e^-}\end{pmatrix}=[r]_{sa}a_1^+. \tag{C1}$$

Now, applying (B2), relationships between the reflected energy flows and the incident energy flows carried by the incident longitudinal wave are determined as

$$\begin{pmatrix} P_l^- \\ P_f^- \end{pmatrix}_l = [R]_{22} \begin{pmatrix} P_l^+ \\ P_f^+ \end{pmatrix}_l . \tag{C2}$$

The subscript l following the vectors indicates that these energy flows are obtained for an incident longitudinal wave. Let us recall that in (C2) the unknowns are the coefficients of the matrix $[R]$. In a same way, another relationship is derived by considering an incident flexural propagating wave instead of a longitudinal wave. Then

$$\begin{pmatrix} P_l^- \\ P_f^- \end{pmatrix}_f = [R]_{22} \begin{pmatrix} P_l^+ \\ P_f^+ \end{pmatrix}_f . \tag{C3}$$

Both (C2) and (C3) provide all the material necessary to calculate the four coefficients of the matrix $[R]$. A numerical verification shows that for a undamped system (evanescent waves do not carry any energy flow), the sum of each column of $[R]$ is equal to one. This fact is relevant to a nondissipative end.

Finally, the reflection efficiencies for either longitudinal or flexural model are just the diagonal coefficients of the matrix $[R]$:

$$r_l = R_{1,1} \quad \text{and} \quad r_f = R_{2,2} . \tag{C4}$$

[1] R. H. Lyon, *Statistical Energy Analysis of Dynamical Systems: Theory and Applications* (MIT, Cambridge, 1975).

[2] E. H. Dowell and Y. Kubota, ''Asymptotic Modal Analysis and Statistical Energy Analysis of Dynamical Systems,'' J. Appl. Mech. **52**, 949–957 (1985).

[3] S. M. Doherty and E. H. Dowell, ''Experimental study of asymptotic modal analysis applied to a rectangular plate with concentrated masses,'' J. Sound Vib. **170**, 671–681 (1994).

[4] J. L. Guyader, ''Modal sampling method for the vibration study of systems of high modal density,'' J. Acoust. Soc. Am. **88**, 2269–2276 (1990).

[5] V. D. Belov, S. A. Rybak, and B. D. Tartakovski, ''Propagation of vibrational energy in absorbing structures,'' J. Sov. Phys. Acoust. **23**, 115–119 (1977).

[6] E. Luzzato, ''Approximations and solutions of the vibration energy density equations in beams,'' Inter Noise 1991.

[7] D. J. Nefske and S. H. Sung, ''Power flow finite element analysis of dynamic systems: Basic theory and applications to beams,'' Statistical Energy Analysis **3**, 47–54 (1987).

[8] J. C. Wohlever and R. J. Bernhard, ''Mechanical energy flow models of rods and beams,'' J. Sound Vib. **153**, 1–19 (1992).

[9] O. M. Bouthier and R. J. Bernhard, ''Simple models of energy flow in vibrating membranes,'' J. Sound Vib. **182**, 129–147 (1995).

[10] O. M. Bouthier and R. J. Bernhard, ''Simple models of the energetics of transversely vibrating plates,'' J. Sound Vib. **182**, 149–164 (1995).

[11] L. S. D. Morley, ''Elastic waves in a naturally curved rod,'' Q. J. Mech. Appl. Math. **14**, (1961).

[12] L. Cremer and M. Heckl, *Structure Born Sound: Structural Vibrations and Sound Radiation at Audio Frequencies* (Springer-Verlag, Berlin, 1973).

[13] Y. Lase and L. Jezequel, ''Analysis of a dynamic system based on a new energetic formulation,'' International Congress on Intensity Techniques, Senlis CETIM (1990).

[14] M. Djimadoum and L. Guyader, ''Prediction of coupled beam energy with the equation of diffusion-boundary, excitation and coupling conditions,'' International Congress on Intensity Techniques, Senlis CETIM (1993).

[15] M. N. Ichchou, ''Formulations énergétiques pour l'étude des moyennes et hautes fréquences des systèmes: Théorie et applications,'' Thèse École Centrale de Lyon No. 96-10.

[16] A. Le Bot and L. Jezequel, ''Energy methods applied to transverse vibrations of beams,'' International Congress on Intensity Techniques, Senlis CETIM (1993).